skb.se

# SKB P-25-10

ISSN 1651-4416
ID 2096103
December 2025

# Scanning surface geometries of fracture intercepts in borehole KFM24

Martin Stigsson, SKB
Magnus Herbertsson, RISE
Michael Kröhn, GRS
Erik Lindvall, RISE
Jörgen Spetz, RISE

*Keywords:* Forsmark, Geometry scanning, Laser scanning, Fracture surface, Scanner tool comparison, KFM24, AP SFK-25-015.

# Summary

A pilot test to scan the surface geometry of fractures intersecting borehole KFM24 was performed. Eleven intercepts were chosen to be a representative sample for the test. The surfaces were scanned by RISE and GRS using four different types of tools. Using different tools and executers adds to the knowledge of best practice when scanning geometry, which will serve as the foundation for the development of a method description. However, the data retrieved may be used for other purposes in the future as well.

The conclusion was that scanning of borehole intercepts usually were easy to perform and faster than expected. After postprocessing the scanned surfaces, the geometries were saved as stereolithography files and stored in the file archive of the Sicada database as activity type GE114.

# Sammanfattning

Ett pilottest för att skanna ytgeometrin på sprickor som korsar borrhål KFM24 har utförts. Elva sprickor valdes ut som ett representativt urval för testet. RISE och GRS skannade ytorna och totalt testades fyra olika verktyg. Genom att använda olika verktyg och utförare ökas kunskapen om bästa sätt att skanna ytgeometri, vilket ligger till grund för framtagandet av en metodbeskrivning. Insamlade data kan dock även användas för andra ändamål i framtiden.

Slutsatsen av testet är att skanningen av sprickor i borrkärnor vanligtvis är enkla att skanna och gick fortare än förväntat. Efter att de skannade ytorna efterbearbetats levererades geometrierna som stereolithography-filer och sparades i Sicadadatabasens filarkiv under aktivitetstypen GE114.

# Content

**1 Introduction ..... 3**

**2 Method and execution ..... 4**
2.1 Preparatory work ..... 4
2.2 Scanning at RISE ..... 9
2.2.1 Artec ..... 9
2.2.2 Leica ..... 12
2.3 Scanning at GRS ..... 14
2.4 Output ..... 19

**3 Summary and conclusions ..... 20**

**4 References ..... 21**
Appendix A. Suggested fractures during desktop study ..... 22
Appendix B. Selected fracturesfeatures for scanning. ..... 23
Appendix C. Visualisation of scanned surfaces using Artec Spider ..... 24
Appendix D. Visualisation of scanned surfaces using Artec EVA ..... 28
Appendix E. Visualisation of scanned surfaces using Leica Absolute Tracker AT960-LR (long range) together with Leica Absolute Scanner ..... 29
Appendix F. Visualisation of scanned surfaces using optical Hexagon 3D-scanner SmartScan-HE R12 ..... 31

# 1 Introduction

Fracture surface roughness and distribution of voids are important parameters for rock mass strength as well as flow and transport of solutes through fractured crystalline rock. The roughness may be retrieved by scanning the surfaces of a fracture, while the voids require the surface scans to be done in a common coordinate system of the two surfaces. Voids may also be approximated by scanning two opposite surfaces and aligning them afterwards.

The purpose of this activity is to examine the usefulness of different laser scanning tools that can serve as the foundation for writing a “Method description” (Metodbeskrivning) on scanning of fracture geometries. Scanning fracture surfaces intersecting cores geometrically may be source to more objectively infer joint roughness.

The activity makes use of four different tools and two different executors to gain knowledge from different ways of performing the geometry scanning. Consequently, there is no method description for the activity, and instead the work was carried out following the “Activity plan” (Aktivitetsplan), AP SFK-25-015, only.

# 2 Method and execution

The work was carried out in two sessions, one at RISE, Research Institute of Sweden, in Borås (May 5 to 6 2025) and one at GRS, Gesellschaft für Anlagen- und Reaktorsicherheit gGmbH, in Braunschweig (September 2 to 3 2025). Both executors scanned the same eleven fracture surfaces intersecting the core of borehole KFM24.

## 2.1 Preparatory work

A desktop study was first performed to select potentially interesting fracture intersections. The study made use of the Sicada table p_fract_core together with the OPTV filmed borehole wall. From this study twelve fracture intercepts, listed in Appendix A, were chosen as possible candidates.

The proposed fracture intercepts were confirmed, or changed, during a visual inspection of the core in Llentabhallen at Forsmak:

- The fracture at borehole length 72.095 m was overcored and had to be skipped. Instead, a fracture at borehole length 69.443 m was chosen.
- The proposed fracture at borehole length 279.703 m was found located in a swarm of broken fractures, and hence, no large surface was available. Instead, an artefact, i.e. a non-natural fracture, in a pegmatite at borehole length 275.890 m was chosen as an alternative and complement to the natural fractures.
- The last part of the core was not available at the field visit and therefore the twelfth suggested fracture was skipped.

The visual inspection at site resulted in eleven fracture intercepts, listed in Table 2-1 and Appendix B, and shown in Figure 2-1 to Figure 2-11.

After registration in the core mapping software Boremap, the 27 core pieces (some intersections consist of several pieces) corresponding to the fractures were packed in two core boxes for transportation to the executors of scanning.

**Table 2-1 The selected fractures in KFM24 and their mapped parameters.**

| SAMPLE # | ADJUSTED SECUP (m) | APERTURE (mm) | MINERAL 1 | MINERAL 2 | MINERAL 3 | ROUGHNESS | SURFACE | STRIKE (°) | DIP (°) | ALPHA (°) | SPECIFIC CAPACITY ($m^2/s$) |
|---|---|---|---|---|---|---|---|---|---|---|---|
| 1 | 69.443 | 0.5 | Chlorite | - | - | Planar | Rough | 70.7 | 78.7 | 17.0 | - |
| 2 | 104.730 | 0.5 | NO DETECTABLE MINERAL | | | Stepped | Rough | 97.9 | 14.0 | 79.3 | - |
| 3 | 126.605 | 2.0 | Chlorite | - | - | Planar | Rough | 295.1 | 35.8 | 50.8 | $2.9 \cdot 10^{-8}$ |
| 4 | 174.030 | 0.0 | Chlorite | Calcite | Striated surfaces | Undulating | Slicken-sided | 348.8 | 77.4 | 15.1 | - |
| 5 | 195.058 | 1.0 | Chlorite | Iron Hydroxide | Oxidized Walls | Stepped | Smooth | 236.3 | 13.5 | 69.7 | $1.6 \cdot 10^{-7}$ |
| 6 | 232.329 | 22.0 | Chlorite | Calcite | - | Planar | Smooth | 213.6 | 21.7 | 61.6 | $1.0 \cdot 10^{-8}$ |
| 7 | 248.466 | 0.5 | Calcite | Chlorite | - | Planar | Smooth | 93.5 | 9.8 | 83.9 | - |
| 8 | 261.042 | 1.0 | NO DETECTABLE MINERAL | | | Planar | Smooth | 89.5 | 8.9 | 85.0 | $9.2 \cdot 10^{-9}$ |
| 9 | 275.890 | Artefact | Pegmatite | - | - | - | - | - | - | - | - |
| 10 | 297.326 | 0.5 | Chlorite | Calcite | - | Undulating | Smooth | 223.8 | 4.2 | 78.1 | $6.0 \cdot 10^{-10}$ |
| 11 | 370.164 | 0.5 | Calcite | Pyrite | - | Planar | Rough | 37.4 | 83.7 | 13.5 | $1.5 \cdot 10^{-9}$ |

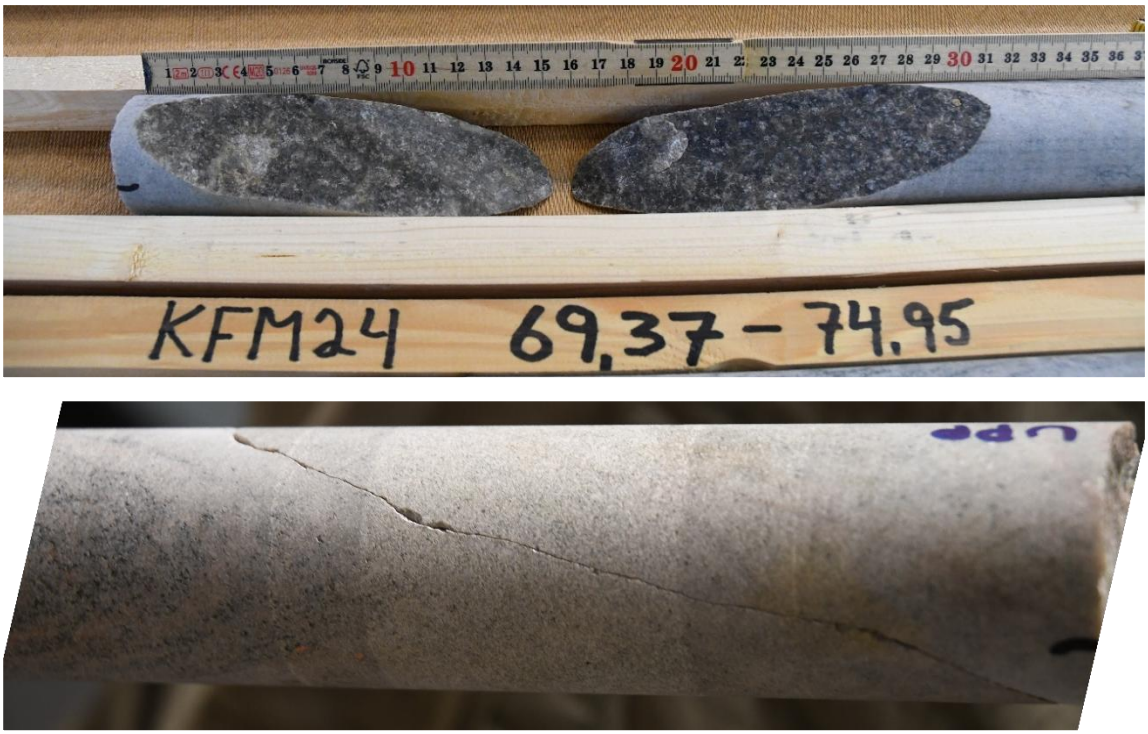


***Figure 2-1.*** *Sample #1 at adjusted secup 69.44 m.*

***Figure 2-2.*** *Sample #2 at adjusted secup 104.73 m.*


***Figure 2-3.*** *Sample #3 at adjusted secup 126.61 m.*

***Figure 2-4.*** *Sample #4 at adjusted secup 174.03 m.*

***Figure 2-5.*** *Sample #5 at adjusted secup 195.06 m.*

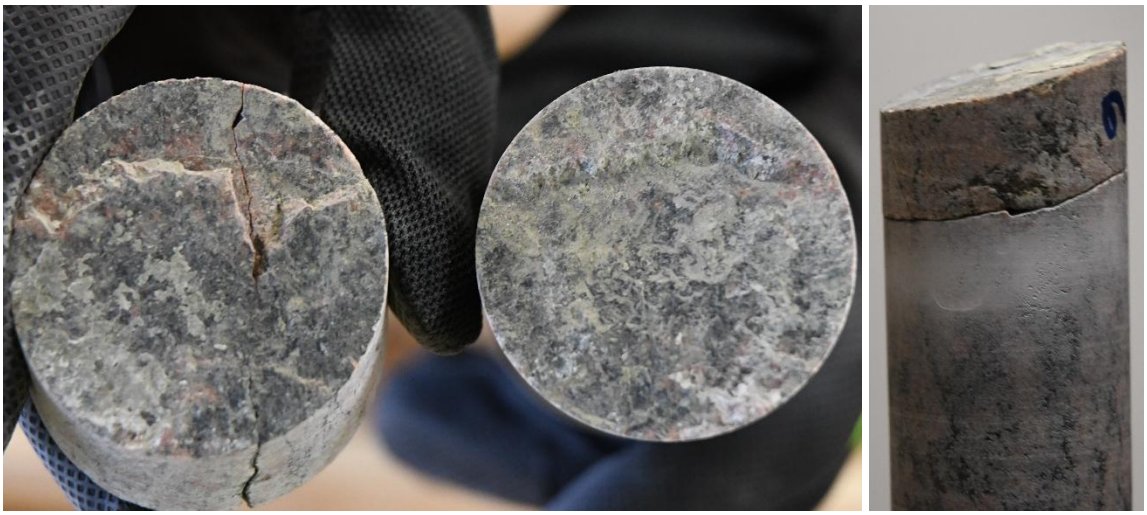

***Figure 2-6.*** *Sample #6 at adjusted secup 232.33 m.*

***Figure 2-7.*** *Sample #7 at adjusted secup 248.47 m.*

***Figure 2-8.*** *Sample #8 at adjusted secup 261.04 m.*

***Figure 2-9.*** *Sample #9 at adjusted secup 275.89 m.*

***Figure 2-10****. Sample #10 at adjusted secup 297.33 m.*

***Figure 2-11.*** *Sample #11 at adjusted secup 370.16 m.*

## 2.2 Scanning at RISE

The core boxes were transported by car to RISE office in Borås. At RISE, tools from two manufacturers were tested, Artec and Leica.

All surfaces, but the small loose piece of sample 3, Figure 2-3, were scanned using the Artec Spider and, as a demonstration, the tool Artec EVA was tested on sample 1.

Leica Absolute Tracker AT960-LR (long range) together with Leica Absolute Scanner were set up in a prototype testbench where sample #1, #3, #4, #7 and #11 were possible to scan.

### 2.2.1 Artec

The Artec Spider (Artec 2025a, 2025b) and EVA (Artec 2025c, 2025d), Figure 2-12, are handheld tools that are relatively fast in scanning the surfaces. It takes 10 to 15 minutes from the time the core is retrieved from the core box until it is returned, including some basic postprocessing of the scan. The actual scan of the surface takes about 1 to 2 minutes for the easy surfaces. The EVA has a lower resolution than the Spider and it also needs to be held farther away from the sample, 0.4 – 1.0 m, compared to the spider, 0.2 – 0.3 m, which makes it harder to use on small samples such as fractures intersecting cores. The EVA is mainly developed for larger objects, > 1dm$^3$. However, it was tested on the two surfaces of sample #1 to show an example of the importance of using tools suitable for the task at hand.

Both tools use structured light technique, which compares the current image and point data in the tool's window with the already gathered image and point data. On the fly, shown on the screen, the software adds the new points building the growing point swarm. This implies that the tool creates its own local coordinate system for each scan, and that the sample can be moved during scanning. This feature was used during the scanning where the short samples were placed on a turntable for easier scanning, Figure 2-13. To facilitate for the software, distinct markers were added on the turntable.

Depending on how shiny the rock minerals are, the surface can be sprayed to matte the shininess, or the sensitivity can be adjusted. Usually, the sensitivity is set to zero, but the shinier fracture surface, the higher sensitivity is necessary. However, increasing sensitivity results in more false points in mid-air. Many of the false points can easily and fast be manually removed, using the tool's software, Figure 2-14. When the manual removal is done the scanning tool's software can automatically remove all remaining points that are not connected to the main surface.

After the basic postprocessing, including removal of mid-air points and points associated with any support structure, Figure 2-15, the scanning tool's software keeps all the useful information of the point cloud internally. From this internal point cloud, the data can be exported as a mesh in an arbitrary resolution, Figure 2-16, to several different formats. For the work carried out, all surfaces were exported as binary stereolithography files, stl, with resolution 0.1 and 0.2 mm using the Artec Spider and 0.2 and 0.5 mm using Artec EVA.

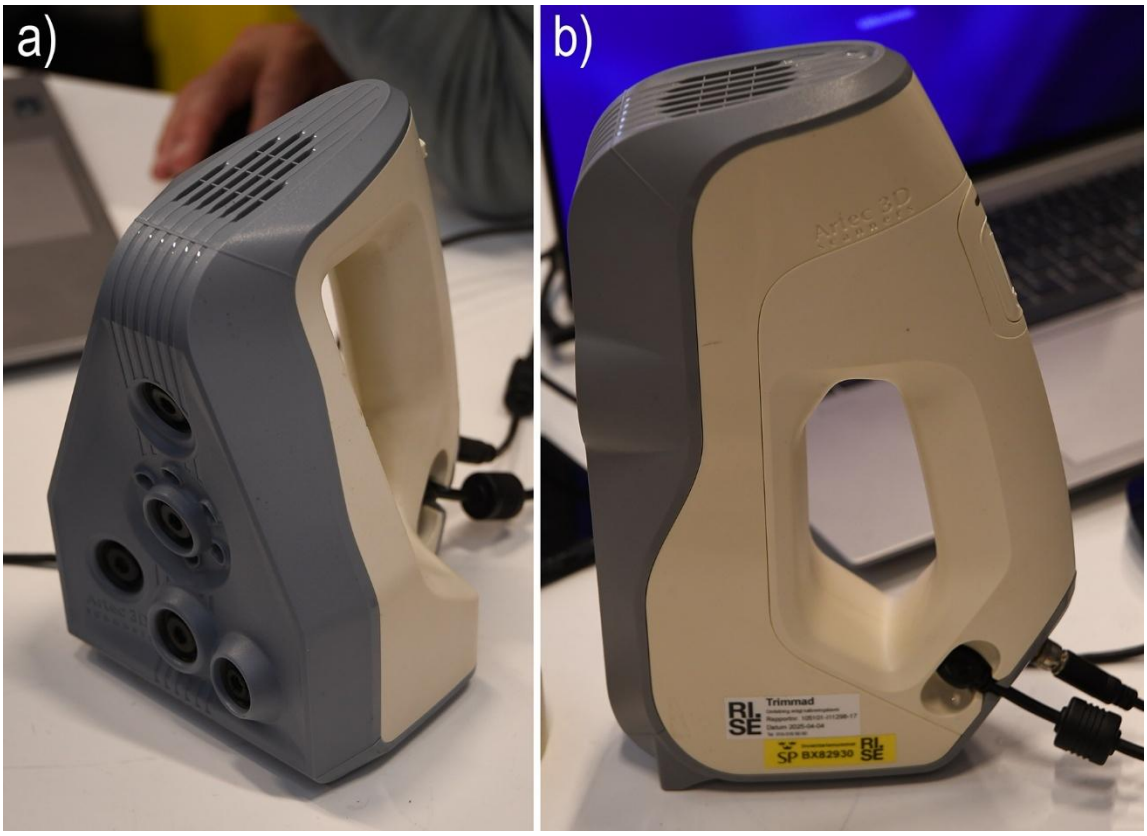


***Figure 2-12.*** *a) Artec Spider, b) Artec EVA.*


***Figure 2-13.*** *Sample #9 ready for scanning. Note the markers, beige tape, on the turntable to facilitate for the scanner to orient and merge the structured light images.*

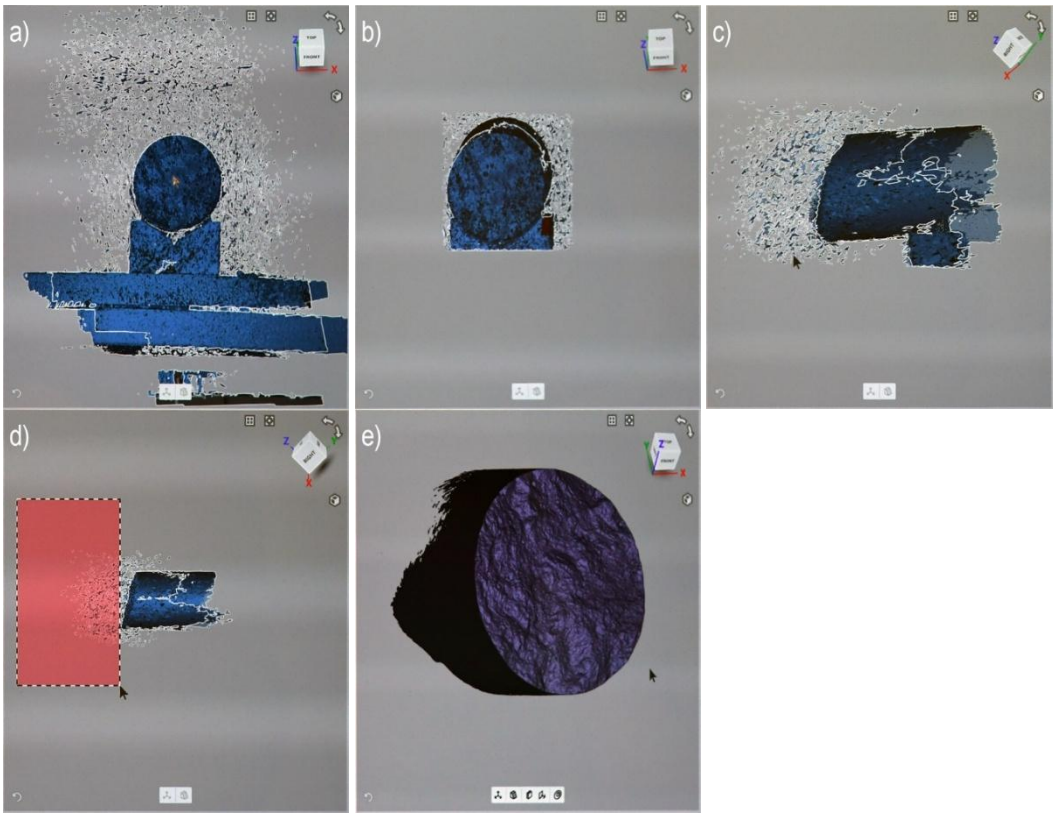


***Figure 2-14.*** *Due to glossy minerals on sample 9 the sensitivity on the Artec Spider had to be increased. a) Lots of mid-air points due to high sensitivity. b) Front view after manually deleting obvious false points. c) Side view of remaining mid-air points. d) Marking of mid-air points. e) Final result, after manual and software removal of unconnected surfaces.*

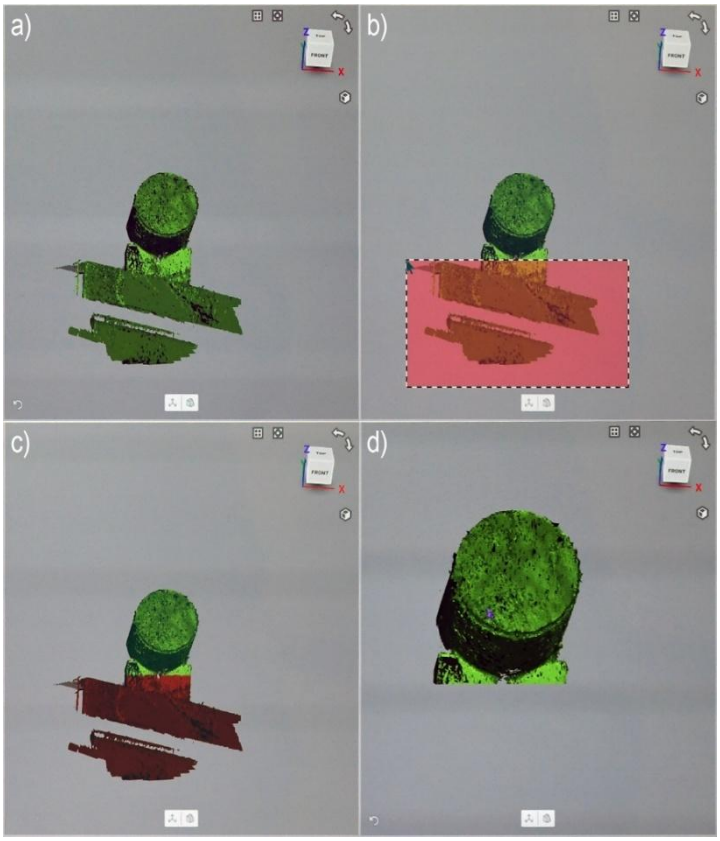


***Figure 2-15.*** *a) Collected vertices and surfaces using Artec Spider. b) Marking of surfaces associated with support structure. c) Selected vertices and surfaces. d) Remaining vertices and surfaces.*

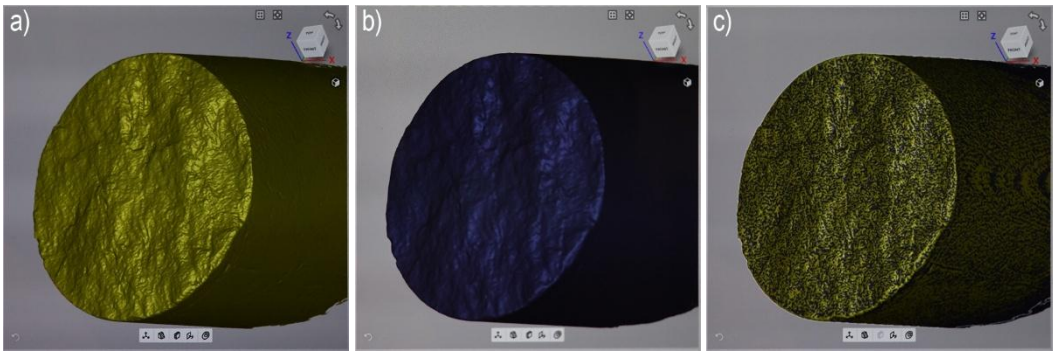


***Figure 2-16.*** *Mesh ‚from Artec Spider, exported with a) 0.1 mm resolution and b) 0.2 mm resolution. c) Overlay of the two meshes where the coarse grid fills the valleys, and the fine grid stands out at the peaks.*

**Some comments to the scanning of the fracture intercepts with Artec Spider as per Table 2-1:**

Sample #1; It was used to test some different settings for the equipment. Results from the visual outcome were that sensitivity should be zero and sharpness set to one as default. Easy to scan.

Sample #2; Easy to scan.

Sample #3; Difficult to scan. Instead of spraying the surface matte, it was decided to try to find settings that still could give good results. Some different settings were tested, but at the end the basic settings were used except that sensitivity was set to 0.7, which resulted in a large number of mid-air points and surfaces. Since the small loose part did not seem to have a unique position, it was decided to skip the scanning of that piece.

Sample #4; Difficult to scan due to parts with shiny minerals. The sensitivity was set to 0.5.

Sample #5; Easy to scan.

Sample #6; Easy to scan. The upper surface was divided into two parts denoted A and B.

Sample #7; Easy to scan.

Sample #8; Easy to scan.

Sample #9; Difficult to scan due to being an induced fracture in a pegmatite having lots of shiny minerals. It was decided to set the sensitivity to 0.5, instead of spraying the surface with a matting substance.

Sample #10; A long core piece, c. 80 cm, that did not fit on the turntable. Otherwise it was easy to scan.

Sample #11; Divided into five pieces, three on the upper surface and two on the lower. All pieces scanned and denoted by increasing letters by decreasing size.

### 2.2.2 Leica

The Leica Absolute Tracker AT960-LR (long range) (Hexagon 2020a) together with the Leica Absolute Scanner (Hexagon 2020b), Figure 2-17, is a combination of a handheld device which is coupled to a stationary unit that keeps track of the absolute position of the scanned object. Hence, it is important that the object subjected to the scanning is fixed in space.

The laser beam of the device swipes fast along a line resulting in a laser line segment projected onto the surface, see Figure 2-18. To get an evenly spread of points on the surface, the line segment must be translated over the surface at a constant low speed perpendicular to the swipe direction. To fulfil this, a prototype, where the scanner was placed on a sleigh that was dragged across the fracture surface, was constructed, Figure 2-19. The test bench was setup in such a way that it could only scan the fracture surfaces from one direction at a fixed angle, and, hence, lacking the possibility to scan from multiple directions, which is essential when scanning rough surfaces. The configuration resulted in a limitation of possible surfaces to scan, i.e. it was difficult to scan surfaces perpendicular to the core and facets with an acute angle to the laser beam. Hence, only surfaces of sample #1, #3, #4, #7 and #11 were scanned.

Once the setup is prepared, the scanning of the fracture surface takes a few minutes depending on the sample length along the scanning direction. The test showed that it is possible to get a good evenly distributed point cloud of the fracture surfaces. However, the surfaces need to be scanned from different directions to be able to generate a good digital elevation model of the surface. A possible development could be to have a hole in the desk where the fracture surface is placed parallel to the desk surface and a system where the sleigh can be pulled in at least four different directions. An alternative to the sleigh, could be to put the scanner on a robot arm that follows a predefined path.

***Figure 2-17.*** *In the rear Leica Absolute Tracker AT960-LR (long range) together with Leica Absolute Scanner in the foreground.*

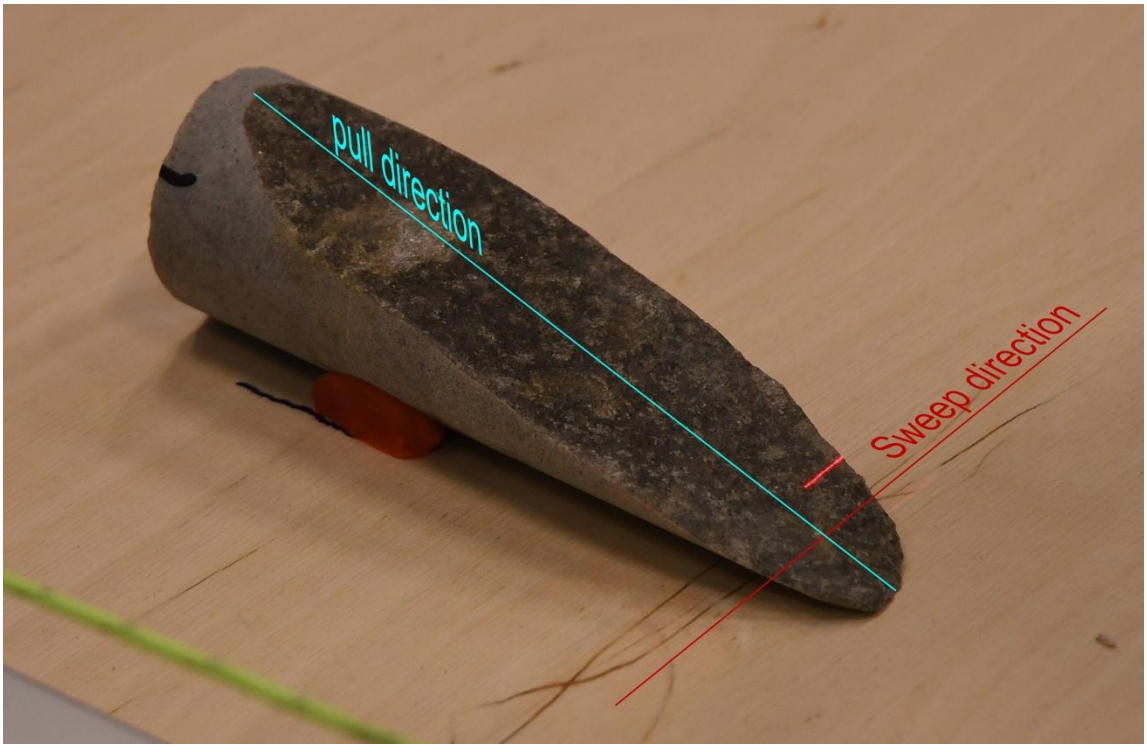


***Figure 2-18.*** *The sweep direction of the laser pulse and the pull direction of the sleigh.*

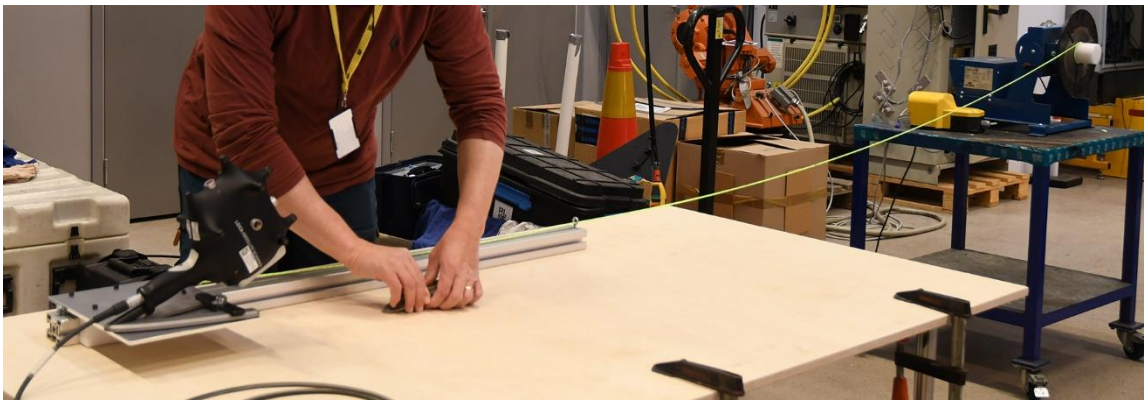

***Figure 2-19.*** *The test bench with the sleigh to the left, and the winding mechanism to the right.*

**Some comments to the scanning of the fracture intercepts with Leica as per Table 2-1:**

Sample #1; The sleigh had to be elevated to be able to run over the sample while scanning the farther parts of the surface. Once rebuilt, the scanning went smooth.

Sample #2; The fracture surface is perpendicular to the core and the core piece is too long to be able to make a useful angle, hence the piece is skipped.

Sample #3; Shiny minerals in combination with acute angles resulting in some small gaps in the digital elevation model.

Sample #4; Some missing facets due to unfavourable angles between the surface and the tool.

Sample #5 and #6; Surface perpendicular to core in combination with too long core pieces make it impossible to scan using the prototype setup.

Sample #7; The down hole lower surface is easy to scan, but the upper surface has an indentation that results in a non-continuous surface.

Sample #8, #9, and #10; Surface perpendicular to core in combination with too long core pieces make it impossible to scan using the prototype setup.

Sample #11; Good results, but a few minor facets missing due to unfavourable angles between the surface and the tool.

## 2.3 Scanning at GRS

The core boxes were transported by car to GRS in Braunschweig, Germany, where the surfaces of all 27 pieces were scanned using an optical Hexagon 3D-scanner SmartScan-HE R12 (Hexagon 2024), Figure 2-20.

The scanner makes use of structured light to determine the geometry of the fracture surfaces. The method works optimal if the surface is non-reflecting, as reflecting surfaces can cause holes in the surface. However, this requirement does usually not correspond well to fracture minerals. Hence, the fracture surfaces are tarnished with a chalk solution, Figure 2-21. As a side benefit of tarnishing, the coating also highlights where the surface suffers from pieces or areas that have partly been detached from the rest of the sample, Figure 2-22. The scanner has aid consisting of two laser devices whose beams are at a slight angle, producing two red dots that align to one for the optimal distance between the scanner head and the sample, Figure 2-22, which allows for quickly finding an optimal focus. When the sample is in focus, the operator is also helped by the scanning tool's software to set, and fine-tune, the exposure time with the help of a colour scale indicator, Figure 2-23. It is possible to combine up to four different exposure times in one single scan to optimize exposure for areas with different colours and brightness.

To acquire the best geometric results, the surface should be scanned almost perpendicular (87°) to the average surface. Due to the rough surface of fractures, it is essential to scan from multiple different directions to measure as many surfaces as possible at a suitable angle in at least one scan. Each single scan takes about 10 seconds and covers a measurement volume of 70 by 55 by 44 mm. Before the scan is accepted by the scanning tool's software, a quality control is performed. Typically, vibrations, flickering of the ambient light sources due to the AC power supply or difficult geometries may lower the quality of the obtained scan. If the surface is rejected by the software the operator may choose to either use the scan anyway or to scan it again from a slightly different angle.

After each scan, the sample is moved a bit so that two consecutive scans show an overlap of about 40%. The new scan is then matched to the already retrieved scans of the surface by the scanning tool's software. Usually this is done automatically, Figure 2-24, but, in some cases, the software requires a rough manual pre-alignment by selecting at least three matching points on the new scan and the existing dataset to guide the software to facilitate the process. The guiding is especially useful for large scans with several hundreds of scans, or when the overlap is small such as scanning over corners and edges.

The scanning tool's software can calculate confidence maps for each scan, depicting the quality of the obtained data visually for the operator as shown in Figure 2-25. Based on this information, the operator can decide to exclude areas with low confidence, when merging the single scans to one common point cloud. The whole data is not deleted, and can, hence, be used later if judged useful in a later stage.

When the scanning is finished, the software OptoCat can automatically realign the surfaces to reduce mismatch, Figure 2-26. After all scans are aligned to satisfaction, the scans can be given different colours to visually check for a reasonable match of the overlapping areas of two scans. The software also enables the operator to manually remove floating elements that are not connected to the scanned surfaces before exporting the fracture surfaces to a desired format. If the surface contains holes they can be stitched as well.

For fracture intercepts that are close to perpendicular to the core axis, and hence less than 20 $cm^2$, ten to fifteen scans are needed to get a good representation of the fracture surface and the rim of the core. The rim is scanned to facilitate the alignment of the two surfaces constructing the fracture. As the angle of an intercept decreases, the fracture area increases and so does the number of needed scans. As an example, it took about 20 minutes from the time the core was retrieved from the core box until it was returned for the two circular intercepts of sample #2, and about 40 minutes for the two oval intercepts of sample #4.


***Figure 2-20.*** *Hexagon 3D-scanner SmartScan-HE R12, mounted on a photogrammetry tripod.*


***Figure 2-21.*** *a) Original fracture surface. b) Sample tarnished using a chalk solution.*

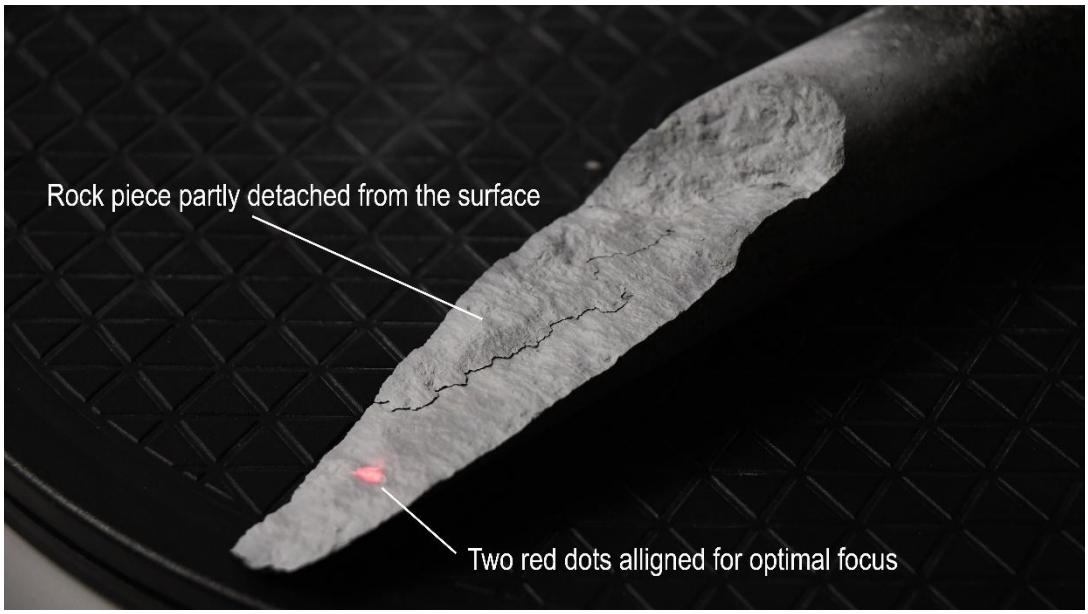


***Figure 2-22.*** *The loose piece is easily spotted when coated with chalk solution. Two red dots are superimposed to get the correct focus for the scanner.*

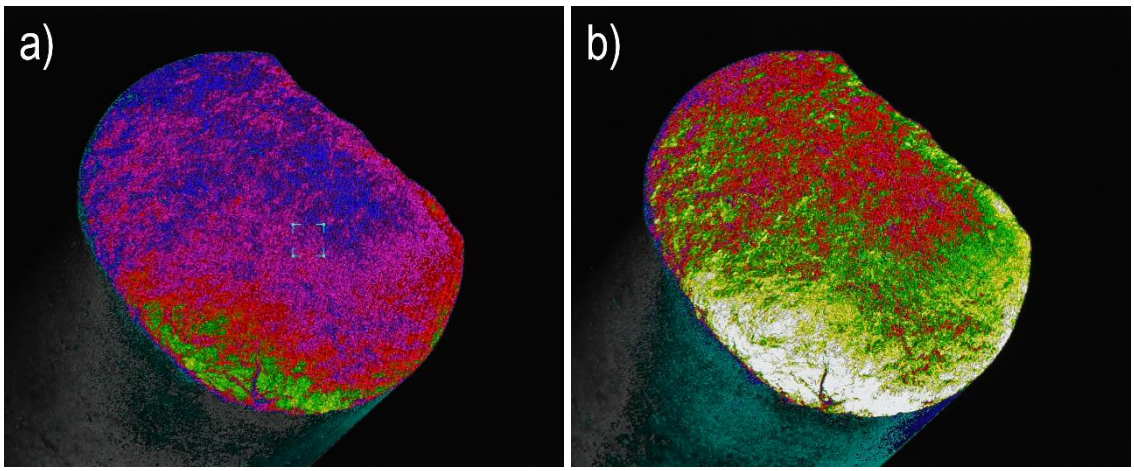


***Figure 2-23.*** *Before the scanning the exposure time is checked. Blue to purple colours indicate under exposure, white to green indicate over exposure, while red reflects optimal exposure time.*

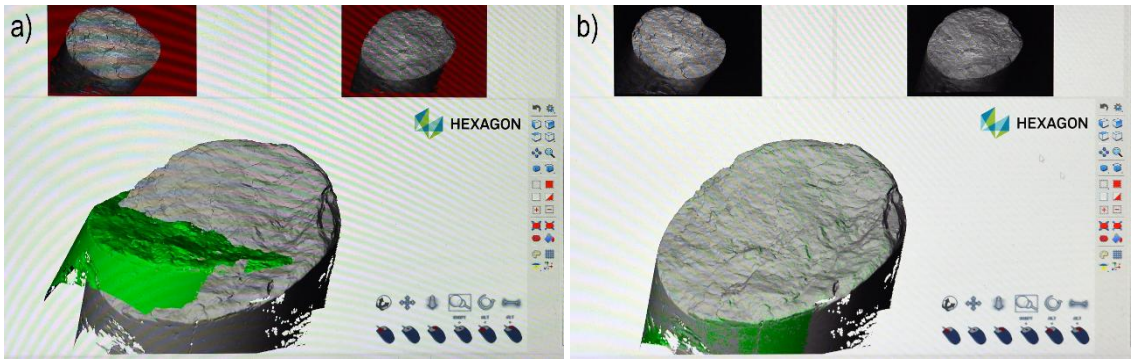


***Figure 2-24.*** *a) New scan, green, together with existing geometry, grey. b) New scan automatically aligned to existing geometry.*

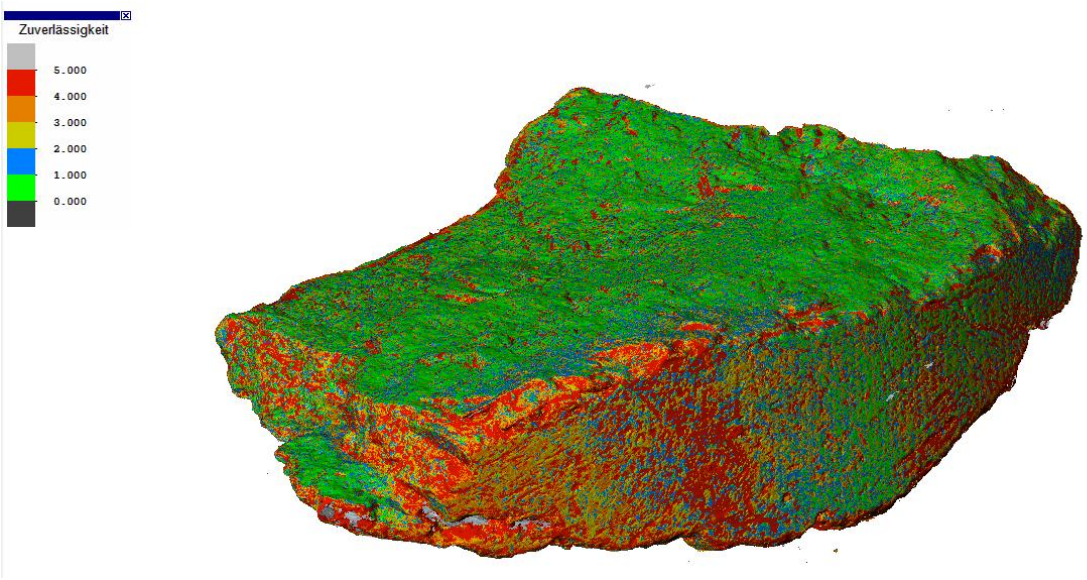


***Figure 2-25.*** *Reliability map showing the quality of the obtained data points, which is derived from the angle between scanner head and element normal. Green colour indicates the highest possible quality while red indicates a low quality.*

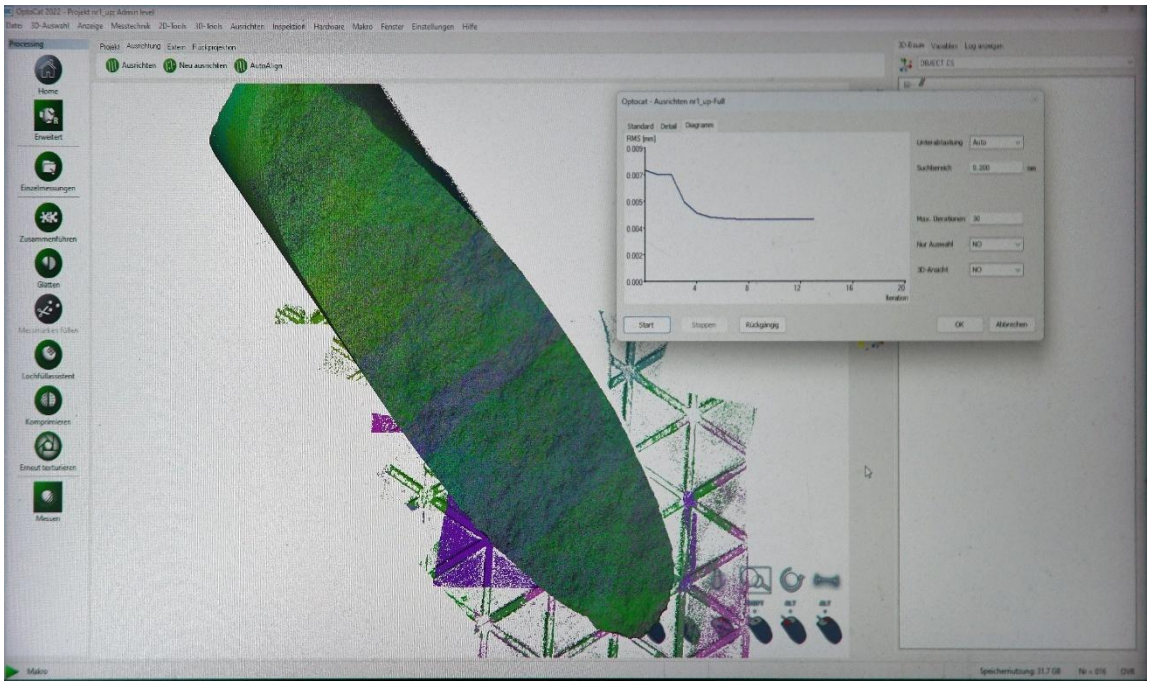

***Figure 2-26.*** *Fine re-alignment of the single scans to each other; plot in the upper right: root mean square error over number of iterations.*

**Some comments to the scanning of the fracture intercepts with SmartScan-HE R12 as per Table 2-1:**

Sample #1; Used to test the different steps when preparing and scanning to see that everything worked as expected. Easy to scan.

Sample #2; Had to find a support to make it stand right up for easier scan. Then easy to scan and done in approximately 20 minutes.

Sample #3; Easy to scan, except for the little loose mid piece, that was difficult to scan around the sharp corners.

Sample #4; Another large fracture. A large semi-detached flake became visible during chalk coating.

Sample #5; A long piece that needed extra support when scanned, still easy to scan.

Sample #6; Easy to scan. The upper surface was divided into two parts denoted A and B, in accordance with previous naming.

Sample #7; Easy to scan.

Sample #8; Easy to scan.

Sample #9; Artefact fracture in a pegmatite sample, easy to scan.

Sample #10; A long core piece, c. 80 cm, that also needed extra support to stand up. Otherwise, it was easy to scan.

Sample #11; Divided into five pieces, three on the uphole surface and two on the downhole surface. All pieces scanned and denoted by increasing letters by decreasing size, in accordance with previous naming.

## 2.4 Output

After the scanning, the surfaces were postprocessed including, for example, deleting floating elements and non-interesting surfaces or adjustment of data with less confidence compared to the rest of the data set. As little postprocessing as possible was performed, i.e. no smoothing or other filters were applied.

The data was then exported as binary stereolithography files for storage in the Sicada database under the activity type (aktivitetstyp) GE114 Scanning geometry of fracture surfaces.

# 3 Summary and conclusions

Most fracture intercepts were easy to scan and both at RISE and at GRS the scanning went faster than expected or scheduled. Hence, the most important lesson learnt is that scanning the fracture surfaces on borehole cores is much easier and faster than scanning larger samples. Despite that most intercepts were easy to scan, a few of them were more difficult, for example, in the cases where the core piece containing the fracture intercept is long or the intercept includes many glossy minerals. During the scanning it was discussed that, it might be possible to speed up the scanning a bit by putting the scanner on a robot arm. However, that demands that the scanning software can exchange information with the robot arm to optimise the movement.

The three scanners tested are developed for reverse engineering, as most other scanners (i.e. create models to be used for manufacturing) or developed for smoother surfaces. This makes it important to scan the fracture surfaces from different angles to capture most of the roughness of the surface. All software coupled to the scanners are powerful to help the operator to find spots with missing data or areas where the data is of less quality. However, it is not always clearly stated what kind of postprocessing the software may perform, that can alter or deform the numerical representation of the geometry of the scanned surface.

This scanning work did not include any comparison of the scanned surfaces using the different scanning tools or techniques. However, a scheme to align the two surfaces of each fracture in a common co-ordinate system was briefly developed and tested with a positive outcome. Hence, it is recommended that such study is performed and reported.

# 4 References

SKB's (Svensk Kärnbränslehantering AB) publications can be found at www.skb.com/publications. SKBdoc documents will be submitted upon request to document@skb.se.


**Artec, 2025a.** Artec Spider II User Manual Version 1.0. Available at: https://docs.artec3d.com/spiderII/User%20Manual/1.0%20Artec%20Spider%20II%20User%20Manual.pdf. [Accessed 2025-11-24]

**Artec, 2025b.** Artec Spider II Technical specifications. Available at: https://www.artec3d.com/portable-3d-scanners/artec-spider#tech-specs. [Accessed 2025-11-24]

**Artec, 2025c.** Artec EVA User's Guide/Manual. Available at: https://docs.artec3d.com/as/17/en/qsg.html#scanning. [Accessed 2025-11-24]

**Artec, 2025d.** Artec EVA Technical specifications. Available at: https://cdn.artec3d.com/content-hub-files/artec-eva-brochure-eng-2023.pdf. [Accessed 2025-11-24]

**Hexagon, 2020a.** Leica AT930/AT960 User Manual. Version 1.2. Available at: https://support.hexagonmi.com/s/article/Leica-Absolute-Tracker-AT930-AT960-User-Manual-v1-2-0en-1528374732805. [Accessed 2025-11-24]

**Hexagon, 2020b.** Leica Absolute Scanner LAS-20-8 User Manual. Version 1.0. Available at: https://support.hexagonmi.com/s/article/Leica-Absolute-Scanner-LAS-20-8-User-Manual-v1-0-0en-1528378300333. [Accessed 2025-11-24]

**Hexagon, 2024.** SmartScan Technical specifications. Available at: https://shop.hexagonmi.com/medias/Hexagon-MI-SLS-SmartScan-data-sheet-A4-en.pdf?context=bWFzdGVyfHJvb3R8NDI2NjQ2fGFwcGxpY2F0aW9uL3BkZnxhR0kzTDJobU5DODVOVFF5T0RneU56SXhPREl5TDBobGVHRm5iMjVmVFVsZlUweFRYMU50WVhKMFUyTmhibDlrWVhSaFgzTm9aV1YwWDBFMFgyVnVMbkJrWmd8MThhZjA2ODNiY2ExYTg3MjliYzRhMjllZWM5YWU2YWJmNDE2NmQ2MzMwZmJjNDJmMWM4NWVmOTI5ZWQwNzkzZg. [Accessed 2025-11-24]

# Appendix A. Suggested fractures during desktop study

**Table A-1. Suggested fractures at the desktop study in KFM24 and their mapped parameters.**

| SAMPLE # | ADJUSTED SECUP (m) | APERTURE (mm) | MINERAL 1 | MINERAL 2 | MINERAL 3 | ROUGHNESS | SURFACE | STRIKE (°) | DIP (°) | ALPHA (°) | FEATURE_ID | SPECIFIC CAPACITY ($m^2/s$) |
|---|---|---|---|---|---|---|---|---|---|---|---|---|
| 1 | 72.095 | 0.5 | Chlorite | | | Planar | Smooth | 116.2 | 59.1 | 33.2 | {3F7C6DE6-D63F-4CDA-9339-256456D00B65} | $1.2E^{-8}$ |
| 2 | 104.730 | 0.5 | NO DETECTABLE MINERAL | | | Stepped | Rough | 97.9 | 14.0 | 79.3 | {3FA9701F-DE9D-4AE5-B413-26C9308B0ABA} | |
| 3 | 126.605 | 2.0 | Chlorite | | | Planar | Rough | 295.1 | 35.8 | 50.8 | {06FB644F-B0F8-46BC-93E4-C3D0272EB415} | $2.9E^{-8}$ |
| 4 | 174.583 | 0.5 | Calcite | Chlorite | Striated surfaces | Undulating | Slickensided | 149.3 | 76.7 | 12.8 | {0D6E319E-6513-4CA9-89A7-56EE612FA390} | |
| 5 | 195.058 | 1.0 | Chlorite | Iron Hydroxide | Oxidized Walls | Stepped | Smooth | 236.3 | 13.5 | 69.7 | {5718EE8D-5A24-4AE2-84E8-ABB993D71442} | $1.6E^{-7}$ |
| 6 | 232.329 | 22.0 | Chlorite | Calcite | | Planar | Smooth | 213.6 | 21.7 | 61.6 | {DDC0822D-8502-4613-AF6C-DBF06092BBBB} | $1.0E^{-8}$ |
| 7 | 248.564 | 0.5 | NO DETECTABLE MINERAL | | | Planar | Smooth | 53.6 | 14.9 | 82.3 | {41ED0927-6270-4533-8F9E-7B8816C0D0C1} | $6.8E^{-9}$ |
| 8 | 261.042 | 1.0 | NO DETECTABLE MINERAL | | | Planar | Smooth | 89.5 | 8.9 | 85.0 | {F767EC0E-E57E-4BA8-9564-5AEC82011A94} | $9.2E^{-9}$ |
| 9 | 279.703 | 0.5 | NO DETECTABLE MINERAL | | | Undulating | Rough | 186.3 | 7.3 | 76.6 | {E81921F8-9FFA-4DE0-96BB-21E634AD3012} | |
| 10 | 297.326 | 0.5 | Chlorite | Calcite | | Undulating | Smooth | 223.8 | 4.2 | 78.1 | {E0F07561-5E57-4853-9993-CBA5340061A1} | $6.0E^{-10}$ |
| 11 | 370.164 | 0.5 | Calcite | Pyrite | | Planar | Rough | 37.4 | 83.7 | 13.5 | {40C8A97E-52B3-4778-8AA9-0E6F618B0D90} | $1.5E^{-9}$ |
| 12 | 414.411 | 1.0 | Chlorite | Pyrite | | Planar | Rough | 38.7 | 82.4 | 14.4 | {86A14624-6612-4656-A7F2-E01CE7D315CA} | $1.4E^{-9}$ |

# Appendix B. Selected fracturesfeatures for scanning.

**Table B-1. Selected fractures for scanning in KFM24 and their mapped parameters.**

| SAMPLE # | ADJUSTED SECUP (m) | APERTURE (mm) | MINERAL 1 | MINERAL 2 | MINERAL 3 | ROUGHNESS | SURFACE | ROCK CODE | STRIKE (°) | DIP (°) | ALPHA (°) | FEATURE_ID | SPECIFIC CAPACITY ($m^2/s$) |
|---|---|---|---|---|---|---|---|---|---|---|---|---|---|
| 1 | 69.443 | 0.5 | Chlorite | - | - | Planar | Rough | 101057 | 70.7 | 78.7 | 17.0 | {AD57EE23-C81D-4CA2-9221-CE9E99FC8012} | - |
| 2 | 104.730 | 0.5 | NO DETECTABLE MINERAL | | | Stepped | Rough | 101057 | 97.9 | 14.0 | 79.3 | {3FA9701F-DE9D-4AE5-B413-26C9308B0ABA} | - |
| 3 | 126.605 | 2.0 | Chlorite | - | - | Planar | Rough | 101057 | 295.1 | 35.8 | 50.8 | {06FB644F-B0F8-46BC-93E4-C3D0272EB415} | $2.9 \cdot 10^{-8}$ |
| 4 | 174.030 | 0.0 | Chlorite | Calcite | Striated surfaces | Undulating | Slickensided | 102017 | 348.8 | 77.4 | 15.1 | {2CE8B216-6C0D-4A2D-826F-30FDCD866C8D} | - |
| 5 | 195.058 | 1.0 | Chlorite | Iron Hydroxide | Oxidized Walls | Stepped | Smooth | 101057 | 236.3 | 13.5 | 69.7 | {5718EE8D-5A24-4AE2-84E8-ABB993D71442} | $1.6 \cdot 10^{-7}$ |
| 6 | 232.329 | 22.0 | Chlorite | Calcite | - | Planar | Smooth | 101057 | 213.6 | 21.7 | 61.6 | {DDC0822D-8502-4613-AF6C-DBF06092BBBB} | $1.0 \cdot 10^{-8}$ |
| 7 | 248.466 | 0.5 | Calcite | Chlorite | - | Planar | Smooth | 101057 | 93.5 | 9.8 | 83.9 | {41ED0927-6270-4533-8F9E-7B8816C0D0C1} | - |
| 8 | 261.042 | 1.0 | NO DETECTABLE MINERAL | | | Planar | Smooth | 101057 | 89.5 | 8.9 | 85.0 | {F767EC0E-E57E-4BA8-9564-5AEC82011A94} | $9.2 \cdot 10^{-9}$ |
| 9 | 275.890 | - | - | - | - | - | - | 101061 | - | - | - | - | - |
| 10 | 297.326 | 0.5 | Chlorite | Calcite | - | Undulating | Smooth | 101057 | 223.8 | 4.2 | 78.1 | {E0F07561-5E57-4853-9993-CBA5340061A1} | $6.0 \cdot 10^{-10}$ |
| 11 | 370.164 | 0.5 | Calcite | Pyrite | - | Planar | Rough | 101057 | 37.4 | 83.7 | 13.5 | {40C8A97E-52B3-4778-8AA9-0E6F618B0D90} | $1.5 \cdot 10^{-9}$ |

ROCK_CODE key

101057: Granite to granodiorite, metamorphic, medium-grained

101061: Pegmatite, pegmatitic granite

102017: Amphibolite

# Appendix C. Visualisation of scanned surfaces using Artec Spider

Fracture #1, ID {AD57EE23-C81D-4CA2-9221-CE9E99FC8012}

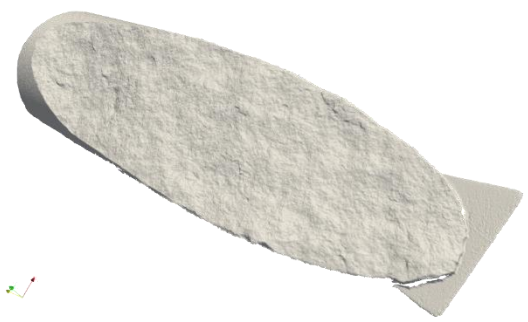

Uphole

Downhole

Fracture #2, ID {3FA9701F-DE9D-4AE5-B413-26C9308B0ABA}

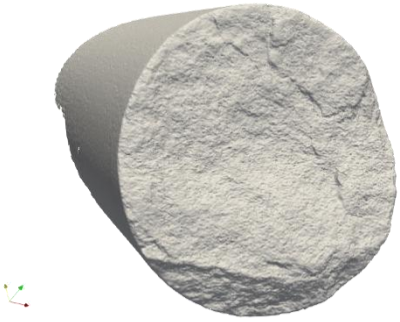

Uphole

Downhole

Fracture #3, ID {06FB644F-B0F8-46BC-93E4-C3D0272EB415}

Uphole

Downhole

Fracture #4, ID {2CE8B216-6C0D-4A2D-826F-30FDCD866C8D}

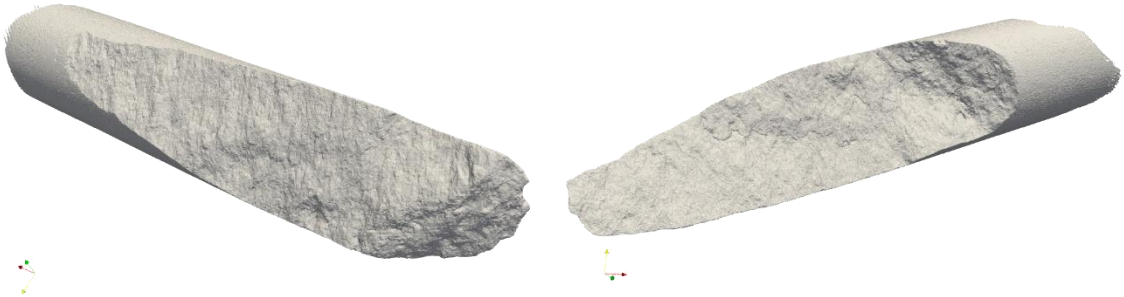

Uphole Downhole

Fracture #5, ID {5718EE8D-5A24-4AE2-84E8-ABB993D71442}

Uphole Downhole

Fracture #6, ID {DDC0822D-8502-4613-AF6C-DBF06092BBBB}

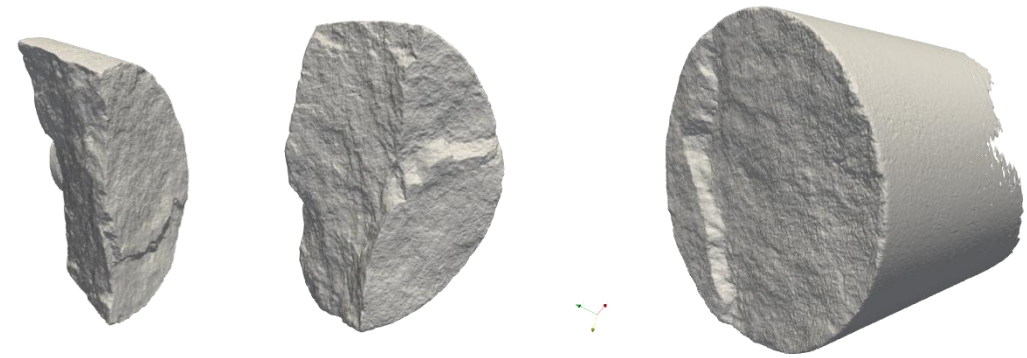

Uphole A Uphole B Downhole

Fracture #7, ID {41ED0927-6270-4533-8F9E-7B8816C0D0C1}

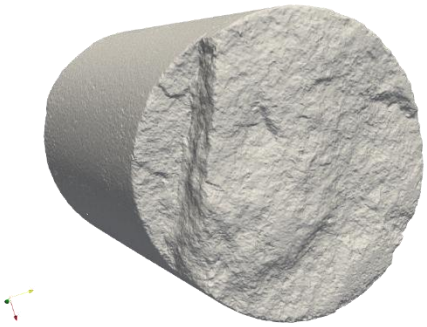

Uphole

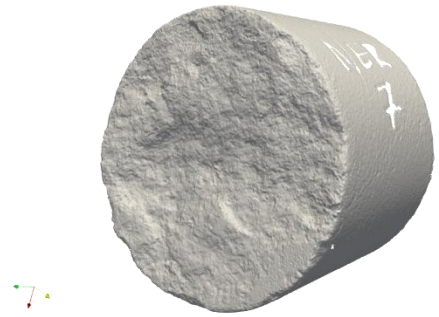

Downhole

Fracture #8, ID {F767EC0E-E57E-4BA8-9564-5AEC82011A94}

Uphole

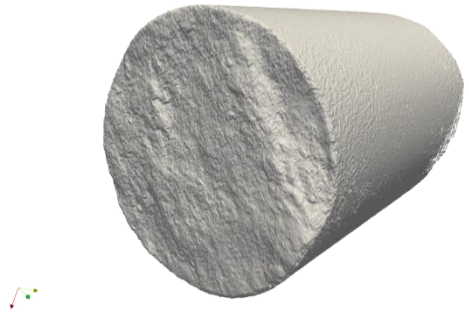

Downhole

Fracture #9, Artefact

Uphole

Downhole

Fracture #10, ID {E0F07561-5E57-4853-9993-CBA5340061A1}

Uphole

Downhole

Fracture #11, ID {40C8A97E-52B3-4778-8AA9-0E6F618B0D90}

Uphole A

Uphole B

Uphole C

Downhole A

Downhole B

# Appendix D. Visualisation of scanned surfaces using Artec EVA

Fracture #1, ID {AD57EE23-C81D-4CA2-9221-CE9E99FC8012}

1 Uphole

1 Downhole

# Appendix E. Visualisation of scanned surfaces using Leica Absolute Tracker AT960-LR (long range) together with Leica Absolute Scanner

Fracture #1, ID {AD57EE23-C81D-4CA2-9221-CE9E99FC8012}

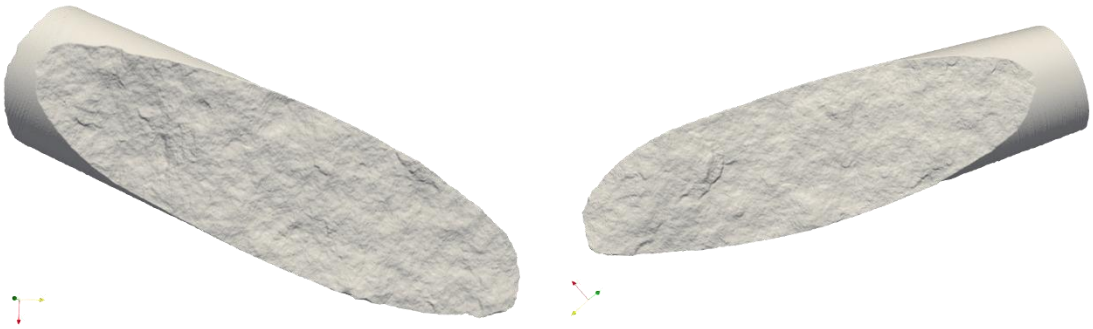

Uphole Downhole

Fracture #3, ID {06FB644F-B0F8-46BC-93E4-C3D0272EB415}

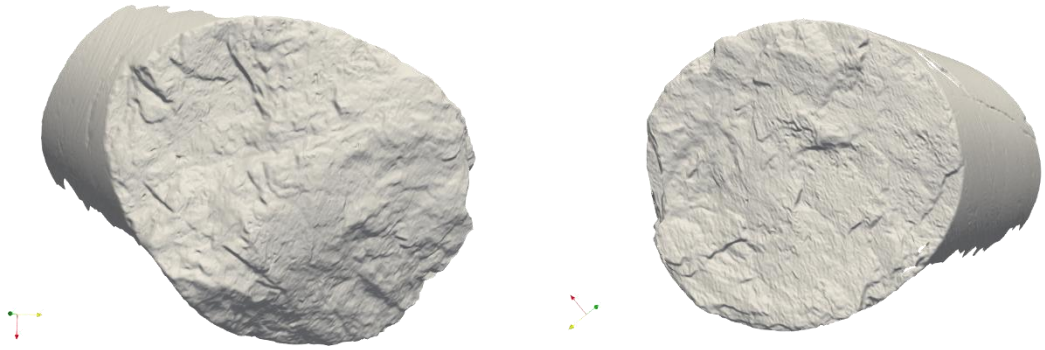

Uphole Downhole

Fracture #4, ID {2CE8B216-6C0D-4A2D-826F-30FDCD866C8D}

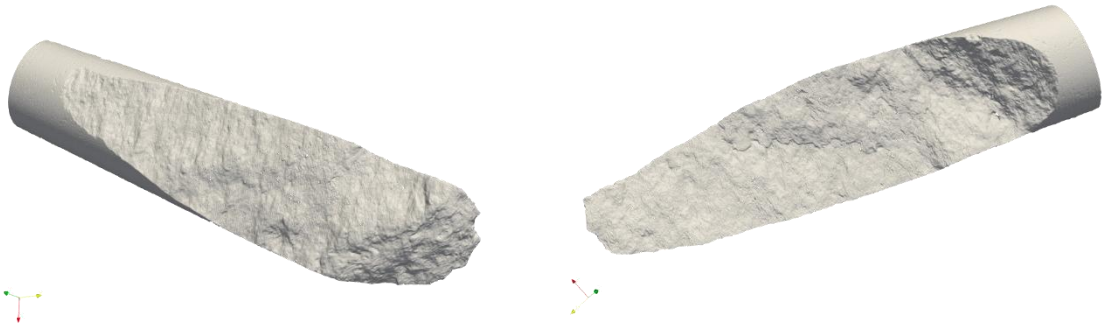

Uphole Downhole

Fracture #7, ID {41ED0927-6270-4533-8F9E-7B8816C0D0C1}

Uphole

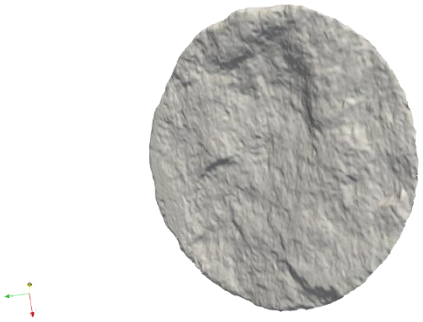

Downhole

Fracture #11, ID {40C8A97E-52B3-4778-8AA9-0E6F618B0D90}

Uphole A

Downhole A

# Appendix F. Visualisation of scanned surfaces using optical Hexagon 3D-scanner SmartScan-HE R12

Fracture #1, ID {AD57EE23-C81D-4CA2-9221-CE9E99FC8012}

Uphole

Downhole

Fracture #2, ID {3FA9701F-DE9D-4AE5-B413-26C9308B0ABA}

Uphole

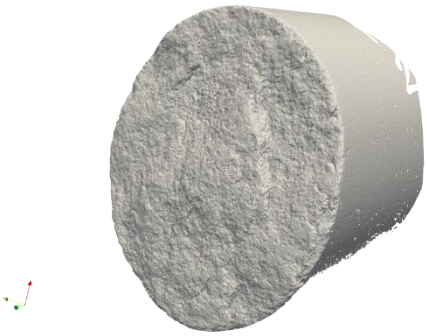

Downhole

Fracture #3, ID {06FB644F-B0F8-46BC-93E4-C3D0272EB415}

Uphole

Downhole

Mid piece

Mid piece

Fracture #4, ID {2CE8B216-6C0D-4A2D-826F-30FDCD866C8D}

Uphole

Downhole

Fracture #5, ID {5718EE8D-5A24-4AE2-84E8-ABB993D71442}

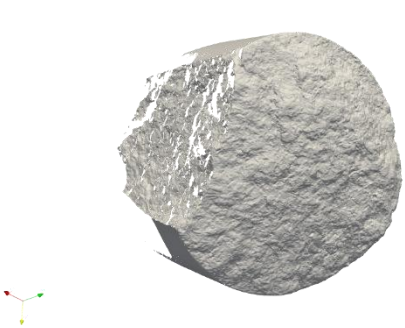

Uphole

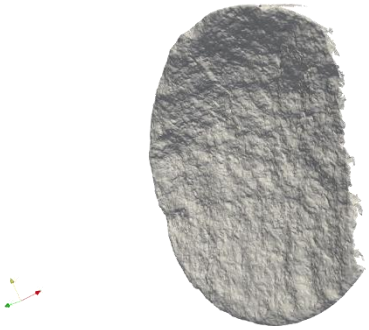

Downhole

Fracture #6, ID {DDC0822D-8502-4613-AF6C-DBF06092BBBB}

Uphole A

Uphole B

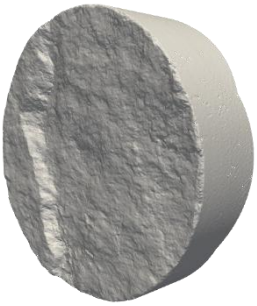

Downhole

Fracture #7, ID {41ED0927-6270-4533-8F9E-7B8816C0D0C1}

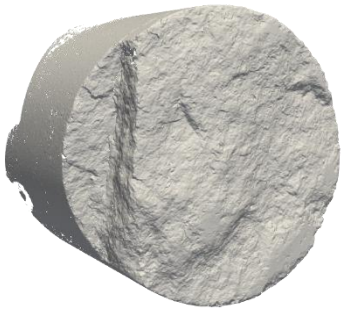

Uphole

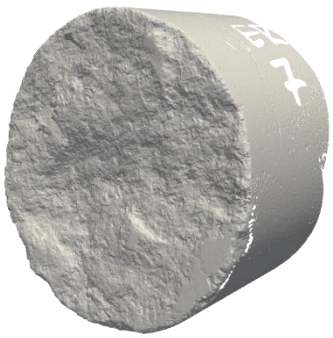

Downhole

Fracture #8, ID {F767EC0E-E57E-4BA8-9564-5AEC82011A94}

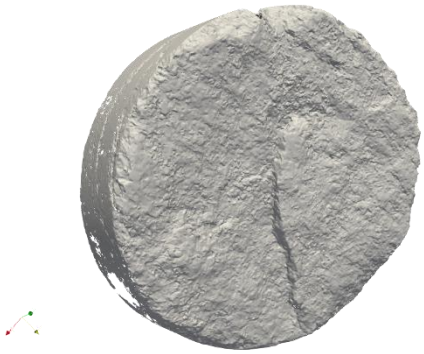

Uphole

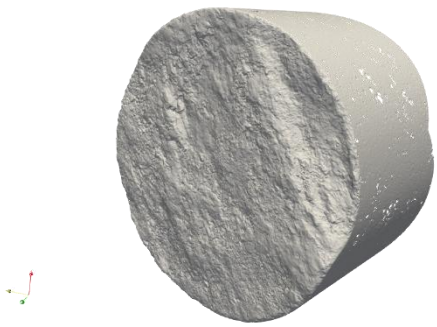

Downhole

Fracture #9, Artefact

Uphole

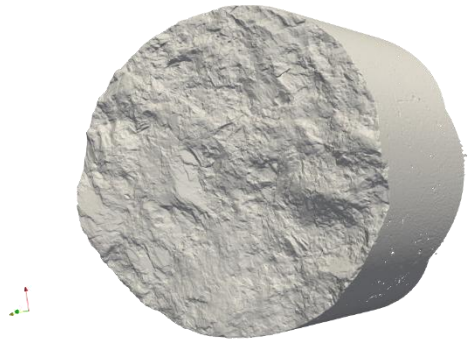

Downhole

Fracture #10, ID {E0F07561-5E57-4853-9993-CBA5340061A1}

Uphole

Downhole

Fracture #11, ID {40C8A97E-52B3-4778-8AA9-0E6F618B0D90}

Uphole A

Uphole B

Uphole C

Downhole A

Downhole B